The Mass of the Atmosphere: A Constraint on Global Analyses

KEVIN E. TRENBERTH AND LESLEY SMITH

National Center for Atmospheric Research, Boulder, Colorado*

(Manuscript received 17 November 2003, in final form 29 June 2004)

ABSTRACT

The total mass of the atmosphere varies mainly from changes in water vapor loading; the former is proportional to global mean surface pressure and the water vapor component is computed directly from specific humidity and precipitable water using the 40-yr European Centre for Medium-Range Weather Forecasts (ECMWF) Re-Analyses (ERA-40). Their difference, the mass of the dry atmosphere, is estimated to be constant for the equivalent surface pressure to within 0.01 hPa based on changes in atmospheric composition. Global reanalyses satisfy this constraint for monthly means for 1979–2001 with a standard deviation of 0.065 hPa. New estimates of the total mass of the atmosphere and its dry component, and their corresponding surface pressures, are larger than previous estimates owing to new topography of the earth's surface that is 5.5 m lower for the global mean. Global mean total surface pressure is 985.50 hPa, 0.9 hPa higher than previous best estimates. The total mean mass of the atmosphere is 5.1480×10^{18} kg with an annual range due to water vapor of 1.2 or 1.5×10^{15} kg depending on whether surface pressure or water vapor data are used; this is somewhat smaller than the previous estimate. The mean mass of water vapor is estimated as 1.27×10^{16} kg and the dry air mass as $5.1352 \pm 0.0003 \times 10^{18}$ kg. The water vapor contribution varies with an annual cycle of 0.29-hPa, a maximum in July of 2.62 hPa, and a minimum in December of 2.33 hPa, although the total global surface pressure has a slightly smaller range. During the 1982/83 and 1997/98 El Niño events, water vapor amounts and thus total mass increased by about 0.1 hPa in surface pressure or 0.5×10^{15} kg for several months. Some evidence exists for slight decreases following the Mount Pinatubo eruption in 1991 and also for upward trends associated with increasing global mean temperatures, but uncertainties due to the changing observing system compromise the evidence.

The physical constraint of conservation of dry air mass is violated in the reanalyses with increasing magnitude prior to the assimilation of satellite data in both ERA-40 and the National Centers for Environmental Prediction–National Center for Atmospheric Research (NCEP–NCAR) reanalyses. The problem areas are shown to occur especially over the Southern Oceans. Substantial spurious changes are also found in surface pressures due to water vapor, especially in the Tropics and subtropics prior to 1979.

1. Introduction

The mass of the atmosphere is of considerable interest in its own right but can also be utilized as a constraint that should be satisfied by global analyses. In this paper we deal with both these aspects. Global analyses of atmospheric fields using four-dimensional data assimilation include as products estimates of surface pressure, water vapor, and hence the mass of dry air. The global mean of the latter is very close to being constant and can be used as a constraint on how well conservation of mass is adhered to as analyses step back in time. A new estimate is made of the mass of the global atmosphere, how it changes during the annual cycle, and its interannual variability.

The total mass of the atmosphere is in fact a fundamental quantity for all atmospheric sciences. It varies in time because of changing constituents, the most notable of which is water vapor. The total mass is directly related to surface pressure while water vapor mixing ratio is measured independently. Accordingly, there are two sources of information on the mean annual cycle of the total mass and the associated water vapor mass. One is from measurements of surface pressure over the globe; the other is from the measurements of water vapor in the atmosphere. New analyses also assess the amount of liquid water in the atmosphere.

However, even the dry atmospheric mass is changing in important ways as humans burn fossil fuels and inject various chemicals and by-products of activities into the atmosphere. Most prominent are changes in carbon dioxide, which has risen from preindustrial estimates of 280 parts per million (ppm) by volume to over 370 ppm

* The National Center for Atmospheric Research is sponsored by the National Science Foundation.

Corresponding author address: Kevin E. Trenberth, National Center for Atmospheric Research, P.O. Box 3000, Boulder, CO 80307.
E-mail: trenbert@ucar.edu

(Houghton et al. 2001). The burning of fossil fuels does not simply add carbon dioxide, however, it also removes oxygen, and so the added mass is 37.5% of the oxygen used. Observations of oxygen concentrations in the atmosphere indeed show that it is declining (Keeling and Shertz 1992; Houghton et al. 2001). The added mass from this process alone would amount to about 0.03 hPa. This is offset by the fact that roughly half of the carbon dioxide generated by fossil fuel burning does not remain in the atmosphere but is taken up by the oceans and biosphere. The latter gives back the oxygen in photosynthesis, while the carbon dioxide entering the ocean may be taken out of the system as carbonate. The net change in mass is likely to be less than 0.01 hPa in surface pressure and is more likely a net loss than a gain in mass. Similarly, outgassing effects and other changes in atmospheric composition typically involve species measured in ppm or parts per billion (Houghton et al. 2001), and thus are even smaller. As we will see, the mass of the atmosphere converted into an equivalent surface pressure is known to within only ~0.1 hPa, and thus these changes are in the noise level and negligible for current purposes.

Nonetheless, precisely because the trace gases are measured in ppm and thus as a mixing ratio, the mass of the atmosphere is needed to convert those values into total amounts. A comprehensive historical review of previous estimates of global, Northern Hemisphere (NH), and Southern Hemisphere (SH) sea level pressures, surface pressures, and the total mass of the atmosphere was given by Trenberth (1981). Since then, several updates have been given using newer datasets and also minor revisions have occurred to more completely take into account the variations in gravity with latitude and height, and the shape of the earth as an ellipsoid. The last full revision by Trenberth and Guillemot (1994) showed that when all factors are taken into account a very good approximation is that

$$m = \frac{2\pi a^2 f}{g} \int_{-\pi/2}^{\pi/2} [p_s(\phi)] \cos\phi \, d\phi,$$

where $f = 1.0020$ is the net effect of the shape of the earth and gravity variations with height and latitude, a=6378.39 km is the equatorial radius of the earth, g = 9.80665 m s^{-2} is the World Meteorological Organization value used for standard gravity at 45° latitude and $[p_s]$ is the zonal average surface pressure. Alternatively, if we use the more common average radius of the earth a = 6371 km then we would use f =1.0043. Numerically this gives $m = 5.22371 \times 10^{15} \, p_s$, where m is the global mean mass in kilograms and here p_s is the global mean surface pressure in hecto-Pascals.

Trenberth and Guillemot (1994) further showed, based on globally analyzed data from the European Centre for Medium-Range Weather Forecasts (ECMWF) for the 4-yr period 1990–93, that the mean annual global surface pressure p_s was 984.76 hPa with a maximum in July of 984.98 hPa and a minimum in December of 984.61 hPa, which correspond to a total mean mass of the atmosphere of 5.1441×10^{18} kg and a range of 1.93×10^{15} kg throughout the year associated with changes in water vapor in the atmosphere. The global annual mean surface pressure due to water vapor p_w was estimated to be 2.4 hPa corresponding to ~2.5 cm of precipitable water. The total atmospheric moisture as given by p_w varied with an annual cycle range of 0.36 hPa, a maximum in July, and a minimum in December. Thus, the mean mass of water vapor was estimated as $1.25 \pm 0.1 \times 10^{16}$ kg and the dry air mass as $5.132 \pm 0.0005 \times 10^{18}$ kg corresponding to a mean surface pressure of $p_d = p_s - p_w = 982.4 \pm 0.1$ hPa.

The above estimates were based upon operational analyses from ECMWF that suffered from continual upgrades and changes in procedures. Since then, past atmospheric data have been reanalyzed by several groups to provide more stable climate global fields of variables. Reanalysis fields for 1948–2002 from the National Centers for Environmental Prediction–National Center for Atmospheric Research (NCEP–NCAR) will be examined here along with those from the 15-yr ECMWF Re-Analysis (ERA-15) from 1979 to 1993, as well as the 40-yr ECMWF Re-Analysis (ERA-40) that runs from mid-1957 to mid-2002. The latter will be the focus of our evaluation and the new estimates of atmospheric mass provided here. Hoinka (1998) evaluated the ERA-15 reanalyses in terms of surface pressure and water vapor contributions and found that the global mean p_s was 984.52 hPa. As previously noted by Trenberth (1981) and Trenberth and Guillemot (1994), such estimates are greatly affected by the global mean orographic height. In meteorology, sea level pressure is the most widely analyzed quantity in weather maps and is robust to modest changes in elevation of the measurement. However, surface pressure is needed for mass computations but its estimated values are affected by the height of the topography. Effectively there is an apparent exchange arising from whether part of the volume above sea level is occupied by solid earth or atmosphere. As shown by Trenberth et al. (1987) and Hoinka (1998), several estimates of the global mean p_s differ because of topography changes in the models used in the analyses, and we will similarly find that substantial changes have again occurred in the latest estimates. We will also present some results from ERA-15 here, but note that these were adversely affected by problems with those reanalyses owing to problems in assimilating satellite data that led to discontinuities in the fields in 1986 and 1989 (Trenberth et al. 2001).

Hence, the revised datasets allow us to provide a new estimate of the mass of the atmosphere and to further examine the water vapor component of the total mass. The total global mass of the dry atmosphere is not constant in the reanalyses, which can be used to show the impact of changes in the observing system with time. We further examine locally where the analyses become

flawed as the database degrades, and the nature of the spurious changes in both surface pressure and water vapor amounts. Then we briefly analyze the monthly mean variability of total mass and thus water vapor mass.

2. Topography and data

The global analyses of surface pressure in four-dimensional data assimilation arise from a blend of observations and a first guess from a numerical weather prediction (NWP) model based on a 6-h forecast in the reanalyses. Owing to limited spatial resolution, the earth's surface in the model does not correspond exactly to that in nature, although this should not affect the spatial average. Moreover, the basic equations in most models do not conserve mass. Typically the equation for total mass conservation (equation of continuity) does not allow for changes in moisture although it should (Trenberth 1991; van den Dool and Saha 1993), and a separate equation tracks the moisture conservation. Most models now have a "mass fixer" to ensure conservation of water vapor and dry air mass after each time step. The missing terms have been incorporated in the NCEP global model since November 1997 (H. van den Dool 2004, personal communication; Wu et al. 1997). However, the main origin of errors in apparent mass conservation comes from the increment in the predicted fields from the new observations, which is not constrained by mass conservation.

In previous analyses of the mass of the atmosphere, errors have been assessed relative to the global mean based on the variability in time. However, the main systematic error in the global mean comes from the height of topography, which has continued to change as improved estimates are made using remote sensing. Trenberth (1981) found that the global mean was 234.9 m using the best available datasets at that time, but this was revised upward to 237.33 m in Trenberth et al. (1987) using a dataset from the U.S. Navy Fleet Numerical Oceanography Center at 1/6° resolution. Values remained near this for a decade, and Trenberth and Guillemot (1994) determined a value of 237.37 m. For ERA-15 Hoinka (1998) gives a value of 238.9 m but this is larger than 237.27 m that we obtain. Small differences can arise from resolution and how global integrals are performed. The global mean height of the topography from NCEP–NCAR and ERA-40 reanalyses is 237.18 and 231.74 m, respectively. Note the marked drop of 5.53 m in the latter relative to ERA-15. In cold conditions, 5.5 m in elevation is equivalent to about 0.75 hPa in p_s. The biggest changes occur over Antarctica and in one area they exceed 1 km in altitude. Airborne laser altimetry is one method leading to improved assessments of altitudes of major ice sheets, and future improvements may occur from instruments on satellites, such as the Ice, Cloud, and Land Elevation Satellite (ICESat) that uses the Geoscience Laser Altimeter System (GLAS) instrument.

The surface pressure due to water vapor is computed from the analyzed specific humidity as

$$p_w = \int_0^{p_s} q \, dp = gw,$$

where w is the precipitable water and q is the specific humidity. These computations were made by ECMWF at full model resolution (T159) in model coordinates using 60 levels in the vertical. All computations of global and regional integrals are performed with Gaussian quadrature and are exact. From the assimilating model, estimates are similarly also made of liquid water.

The reanalyses use a stable analysis and data processing system, but the observations entering the system change with time. Continual changes occur in in situ measurements such as from radiosondes as they are improved and vendors and manufacturers change. Aircraft and ship observations gradually increase over time and are mostly not systematic except that ships report at synoptic times. The main changes, however, are those associated with satellites, which vary in number, have finite lifetimes, and are replaced every few years. There are platform heating effects, instrument degradation, the orbits of satellites decay, and changes occur in local equator crossing times. Of particular note is the introduction of satellite radiances with VTPR in 1973 until 1978 when they were replaced by TOVS (HIRS, MSU, SSU), TOMS, and SBUV (for ozone).[1] Cloud-tracked winds were introduced in 1973. SSM/I surface winds and column water vapor began in 1987 and surface winds from the ERS scatterometer in 1992. ATOVS radiances were introduced on one satellite in 1998 and replaced TOVS entirely in 2001. Not all of these were used in the NCEP reanalyses, for instance the VTPR data were not assimilated. In ERA-40, great care is taken to "bias correct" for all the different instruments by comparing overlapping observations and calibrating them with radiosondes. As a result, the main differences arise when a completely new set of measurements are introduced, most notably the VTPR and TOVS.

3. The global mass and mean annual cycle

Time series of the global mean surface pressure for the total p_s, the water vapor component p_w, and their

[1] Acronyms are as follows: Vertical Temperature Profile Radiometer (VTPR); Television Infrared Observation Satellite (TIROS) Operational Vertical Sounder (TOVS); Advanced TOVS (ATOVS); High Resolution Infrared Radiation Sounder (HIRS); Microwave Sounder Unit (MSU); Stratospheric Sounding Unit (SSU); Total Ozone Mapping Spectrometer (TOMS); Solar Backscatter Ultraviolet (SBUV); European Remote Sensing Satellite (ERS); Special Sensor Microwave Imager (SSM/I).

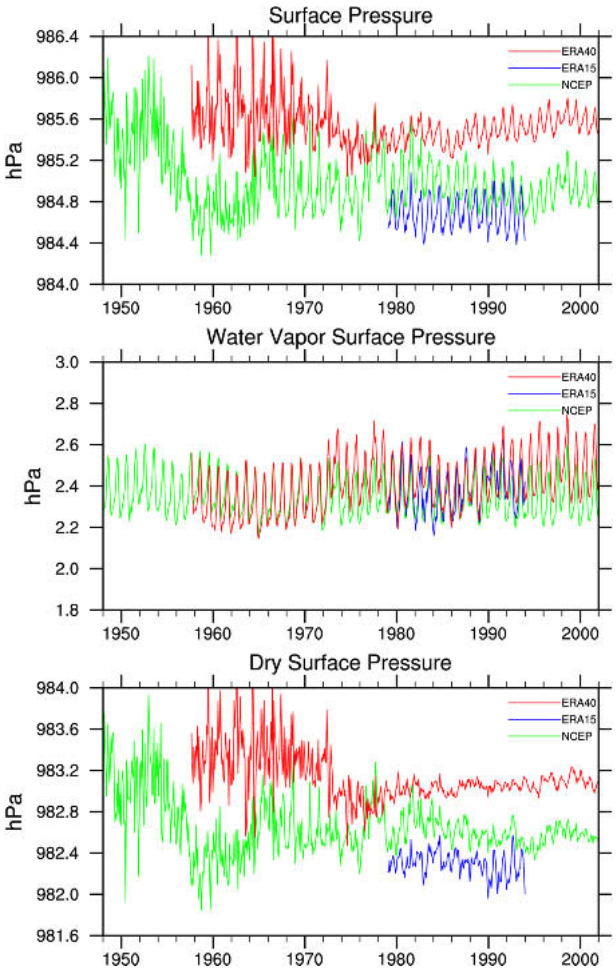

FIG. 1. Time series of global mean surface pressures for (top) the total p_s, and contributions from (middle) water vapor p_w and (bottom) dry air p_d for three different reanalyses from ERA-40 (red), ERA-15 (blue), and NCEP–NCAR (green) in hPa. (middle) The vertical scale is magnified compared to that of the (top) and (bottom).

difference due to dry air p_d, from the three different reanalyses (Fig. 1) show several features of interest. First of note is the offset among different estimates of p_s and p_d, which is mainly caused by the differences in topography discussed in section 2. The second feature of note in the top two panels is the strong annual cycle, which is due to water vapor as it is largely absent in the third panel. The larger amplitude of the annual cycle in p_s for ERA-15 after 1989 shows up in the p_d panel as a spurious feature that is associated with the discontinuities found by Trenberth et al. (2001). The third main feature to note in the ERA-40 and NCEP time series is the increasing amplitude of ragged fluctuations back in time before 1979 in p_s and p_d.

It is apparent (Fig. 1) that the two biggest discontinuities occur in 1973 and 1979 for ERA-40 and in 1979 for NCEP. Judged by the constancy of the lowest panel for p_d, the NCEP reanalyses get progressively noisier prior to the mid-1990s, much more so before 1979, and become quite wild before the mid-1960s. Clearly the VTPR soundings, even though of coarse horizontal resolution (and thus apt to be contaminated by clouds), kept the ERA-40 reanalyses more stable from 1973 to 1978. Before 1973 there is a jump to higher values and with large spurious fluctuations from month to month and year to year. At the same time the water vapor p_w jumps to somewhat lower values. The NCEP water vapor is much more stable throughout (perhaps indicating less influence of the observations).

To determine the mass of the atmosphere, we focus on the post-1979 period for ERA-40, which has the best performance overall in terms of a stable global p_d. We determine the mean annual cycle for this period from each reanalysis and remove it from the entire record, giving the time series (Fig. 2). Note the change in vertical scale for p_w. Even within the time interval after 1979, it is apparent visually that there is a slight increase of p_s relative to the mean after 1994 and unduly low values during ~1985–86. Amazingly, all of these also occur, although to a lesser degree, in p_w and thus are less apparent in p_d, although still slightly in evidence, suggesting they may be mostly real. Moreover, some of the interannual variability in p_w also appears in the NCEP anomalies, notably the increase in 1998 when there was a major El Niño (see section 5).

For completeness we also examined the values of the surface pressure due to total column water other than water vapor, which includes the liquid water and ice, from ERA-40. The values range up to about 300 g m^{-2} (Weng et al. 1997) and global mean surface pressures from ERA-40 are 1.3 Pa, ranging from 0.9 (February) to 1.5 Pa (December). Accordingly, they are small (0.01 hPa) and generally negligible for current purposes.

The values for the mean annual cycle and annual mean are given in Table 1 for ERA-40. For 1979–2001, the mean p_s is 985.50 hPa and for p_d it is 983.05 hPa. Based on the monthly mean anomalies, the standard deviation of the latter is 0.065 hPa. In Table 1 there is a distinctive spurious annual cycle in p_d with peak values in November and December that are 0.11 hPa higher than in June. The 12-month harmonic has an amplitude of 0.05 hPa. Figure 3 presents the mean annual cycle of the two hemispheric means as well as the global mean for all three quantities.

As the average temperature in the NH is larger than the SH, its water holding capacity is also larger and, even though the mean relative humidity is generally less latitude by latitude (the exception being Antarctica), the moisture content is indeed greater in the NH (Trenberth 1981). Further, because of the larger annual cycle in temperature in the NH associated with the greater landmass, which is reflected in moisture holding capacity and actual moisture itself (Trenberth 1981), the maximum in water vapor and thus in total mass occurs in July (for p_w) or August (for p_s) (Table 1; see

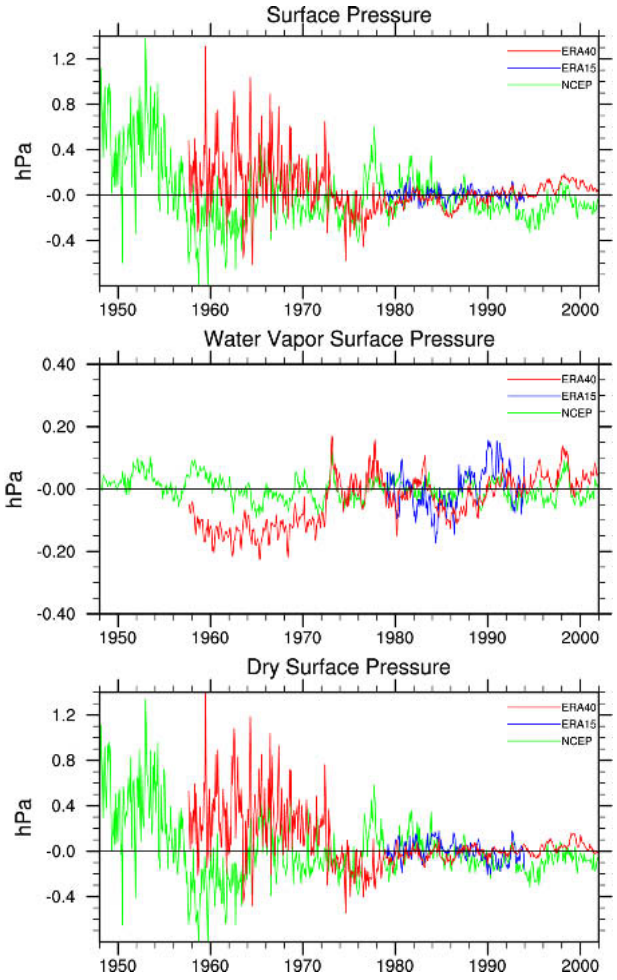

FIG. 2. Time series of global mean surface pressure anomalies relative to 1979–2001 for (top) the total p_s, and contributions from (middle) water vapor p_w and (bottom) dry air p_d for three reanalyses from ERA-40 (red), ERA-15 (blue), and NCEP–NCAR (green) in hPa. Note the amplified vertical scale of the middle panel.

also Figs. 1 and 3). The lowest values occur in January. However, the annual cycle range for p_s is 0.23 versus 0.29 hPa for p_w and the discrepancy is even larger for the 12-month harmonic, which has amplitudes of 0.10 and 0.14 hPa, respectively. Hence either the annual cycle of p_w is too large or that of p_s is too small to satisfy the global constraint of constant p_d. Allowing for this systematic annual cycle error and assuming the rest is random would give the standard error of the mean p_d as 0.035 hPa.

The annual mean p_w is very close to that of Trenberth and Guillemot (1994), given in the introduction, and other independent analyses discussed there. Hence we use the values in Table 1 to estimate new values of mass of the atmosphere. The total mean mass of the atmosphere is 5.1480×10^{18} kg with a range of 1.20×10^{15} kg (for p_s) or 1.51×10^{15} kg (for p_w). The latter are both somewhat smaller than the previous estimate. The mean mass of water vapor is estimated as 1.27×10^{16} kg and the dry air mass as $5.1352 \pm 0.0003 \times 10^{18}$ kg. The error bars here are based on the entire post-1979 record and the random component is somewhat smaller.

The mean annual cycles as a function of latitude and areally weighted by $\cos\phi$, so that the contribution to the global mean can be readily assessed (Fig. 4), reveal that the large annual cycle is associated with the tropical and subtropical monsoons, with higher pressures in the subtropics of the winter hemisphere and an annual amplitude of about 3 hPa near 20°S and slightly less at 20°N. The seasonal migration of dry air across the equator corresponds to a vertical and zonal mean meridional velocity peaking at about 1.5 mm s^{-1}, flowing northward in August–September–October, and southward in April–May–June (Trenberth et al. 1987). The flow of dry air across the equator is compensated by a summertime increase in moisture that has an annual cycle with an amplitude of 0.9 hPa in the NH and 0.7 hPa in the SH near 10°–15° latitude (Fig. 4).

4. Problems prior to 1979

The time series of total mass as equivalent surface pressure (Figs. 1 and 2) reveal problems prior to the satellite era and suspicion immediately falls on the areas of the globe that are not well observed by in situ observations, notably the oceans and especially the SH. Because there is clear evidence that global mass is spuriously higher prior to 1979 in ERA-40, we seek to determine whether the problem areas are pervasive or somewhat localized. The additional spurious variability in Figs. 1 and 2 also suggests that there may be false changes in regional variability. Accordingly, we have carried out exploratory analysis to better isolate the problem areas by using 1979–2001 as a base period for defining means and variability, and examining previous eras of somewhat homogeneous observations for their possible biases.

The zonal mean time series as Hovmöller diagrams for p_s and p_w (Fig. 5) reveal fairly distinctive changes

TABLE 1. Monthly mean values of surface pressure components p_s, p_w, and p_d for 1979–2001 in hPa.

	Jan	Feb	Mar	Apr	May	Jun	Jul	Aug	Sep	Oct	Nov	Dec	Annual
p_s	985.41	985.43	985.46	985.48	985.52	985.55	985.62	985.64	985.54	985.48	985.44	985.43	985.50
p_w	2.33	2.34	2.38	2.44	2.49	2.56	2.62	2.61	2.49	2.39	2.34	2.33	2.44
p_d	983.08	983.09	983.07	983.04	983.03	982.99	983.00	983.03	983.05	983.08	983.10	983.10	983.05

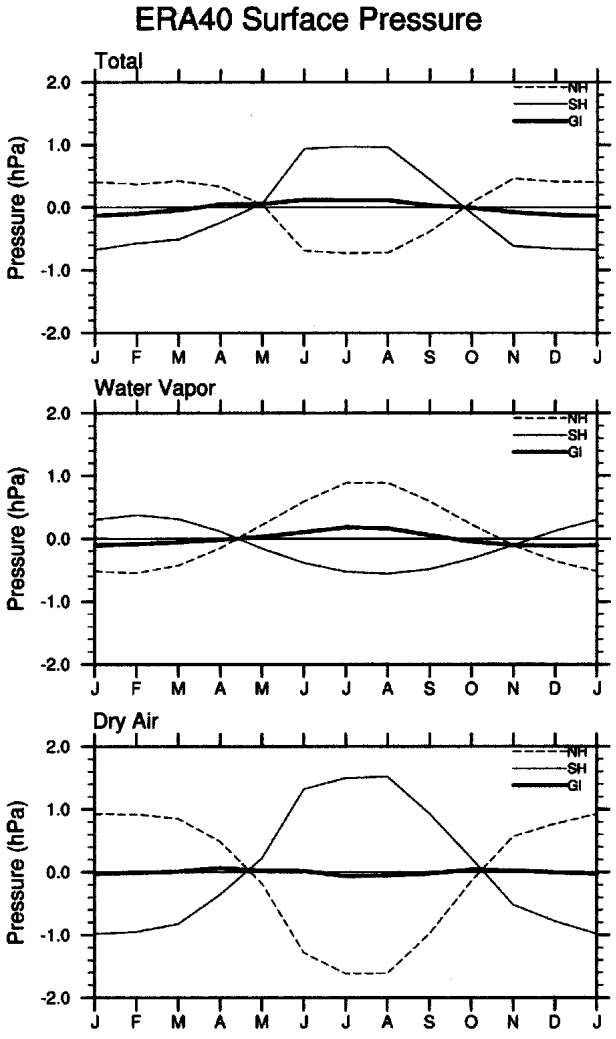

FIG. 3. Mean annual cycle of the hemispheric and global mean surface pressure anomalies relative to 1979–2001 means for (top) the total p_s, and contributions from (middle) water vapor p_w and-(bottom) dry air p_d for ERA-40. The units are in hPa.

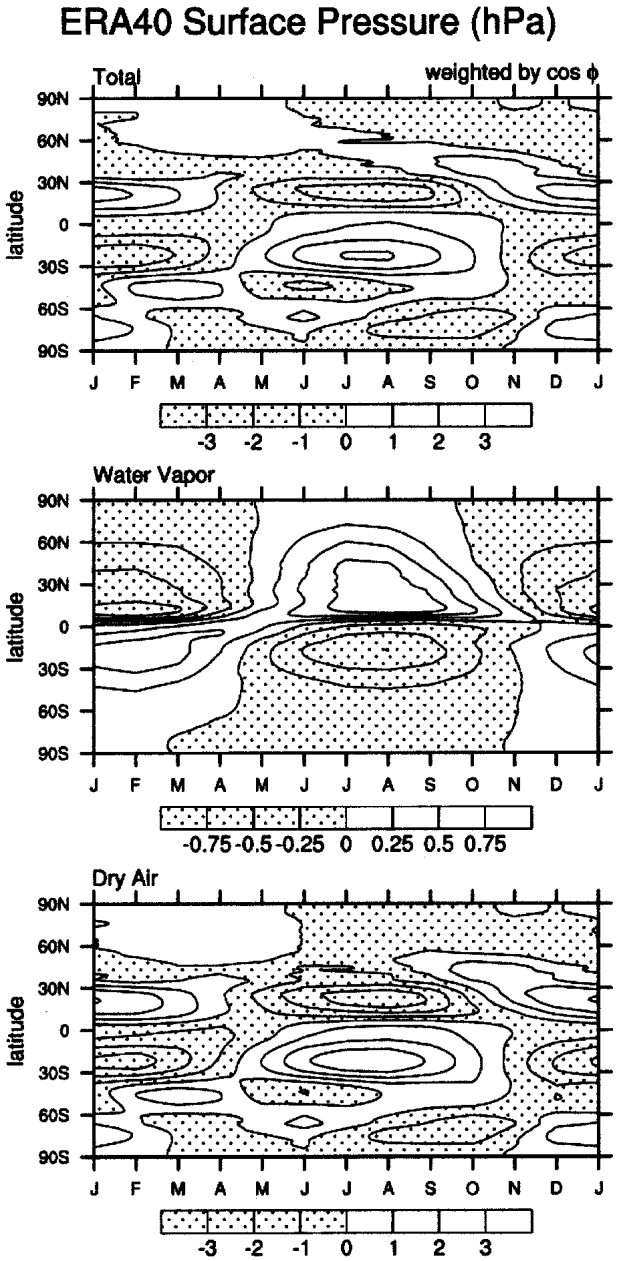

FIG. 4. Mean annual cycle of the mean surface pressure anomalies relative to 1979–2001 means for (top) the total p_s, and contributions from (middle) water vapor p_w and (bottom) dry air p_d for ERA-40. All values are weighted by cosϕ to represent areal weighting and thus depict mass. The units are in hPa.

across the transitions at the beginning of 1973 and 1979. For p_s the main changes are evident as higher values over the Southern Ocean latitudes from 50° to 70°S before 1979. For p_w, the main changes are in the SH subtropics for 1973–78 and Tropics for 1957–72.

As a result we further explored these problems by examining the subperiods 1958–72 and 1973–78 compared with 1979–2001 using a t test for differences in means and an F test for differences in variability. We conservatively assume one degree of freedom for each year. The results for 1958–72 (Fig. 6) reveal the increase in surface pressure around Antarctica as a significant feature as well as possible problems in the high-latitude Arctic region and near Greenland. Lower pressures over parts of the southern Indian Ocean and South Atlantic in December–January–February (DJF) also appear to be suspect. It is surprising how the spuriously high pressures over the Southern Ocean follow the coastline so closely. Water vapor decreases are generally present throughout the deep Tropics but extend over North America and the North Atlantic in June–July–August (JJA). Because radiosonde sensors for water vapor were not very reliable during these times, for instance, prior to 1973 over the United States (Ross and Elliott 1996), the reality of changes must be viewed with

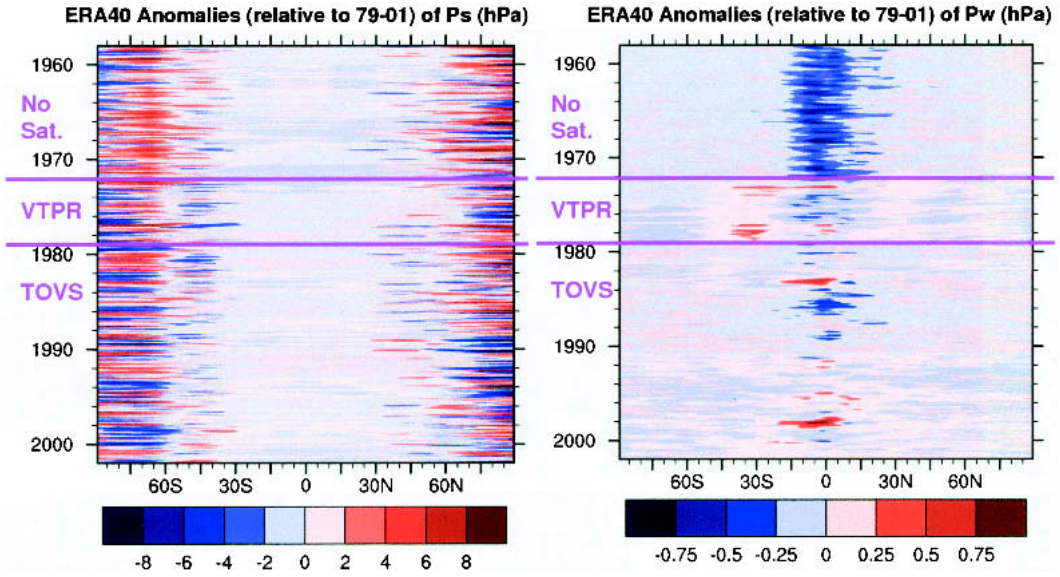

FIG. 5. Latitude–time series of zonal mean surface pressure for (left) the total and (right) water vapor contribution in hPa. The times of transition of the observations from no satellite include VTPR in 1973 and TOVS in 1979.

skepticism even though they extend over regions with observations.

For 1973–78 (Fig. 7) the subperiod is short enough that some features show up as significant but depict real variations in atmospheric circulation, such as those associated with the 1976 climate shift (Trenberth 1990). For instance, the network of observations over New Zealand is adequate to define the climate reliably, and the changes in JJA are no doubt real. Low pressures in DJF again occur over the southern Indian and Atlantic Oceans perhaps indicating they may be real and associated with unduly high values in recent decades. Indeed, evidence is mounting that such changes in the circulation over the SH are hemispheric in extent, associated with the Southern Annular Mode (SAM) and caused at least in part by changes in stratospheric ozone (Gillett and Thompson 2003). However, inadequate sampling of ENSO in such a short period means that changes in the Tropics are aliased. Once again, however, even though often not statistically significant by the measure used, the region right around the coast of Antarctica shows up in a highly suspicious pattern quite like that for the earlier subperiod. This is undoubtedly not real as we can see from the global constraint of conservation of mass, although it is in the sense expected from changes in SAM. Possibly specifications of sea ice coverage and sea surface temperatures in the presatellite era are factors in this behavior in the analyses, in addition to the lack of satellite data. For water vapor, changes are suspicious throughout the Tropics and subtropics, with significant unduly high values in the subtropics and values low over oceanic areas in the deep Tropics, as in the earlier 1958–72 subperiod.

For variance, the tests for changes reveal significant patterns although they seem more likely to be real and associated with the 1976 climate shift and changes in SAM, and hence only samples are shown. Regions of significance occur in the Pacific in DJF (Fig. 8) for both surface pressure and water vapor, with reduced variance in the earlier years. Because the biggest El Niños on record occurred in 1982/83 and 1997/98, this is not surprising. A particular example of changes in variance for 1973–78 JJA is shown in Fig. 9 for surface pressure. Of note is the much larger variance near New Zealand in the 1973–78 subperiod associated with blocking anticyclones (Trenberth and Mo 1985), but that seems to have shifted farther to the southeast in the more recent period (e.g., Renwick and Revell 1999). Again, these changes are mostly, if not entirely, real.

5. Interannual variability

Interannual variations in the total atmospheric mass might be expected as the loading of water vapor increases, for instance, as part of the El Niño phenomenon (e.g., see Gaffen et al. 1991). Similarly, upward trends in water vapor content are anticipated from model studies of "global warming" and climate change associated with increases in greenhouse gases in the atmosphere (Houghton et al. 2001; Trenberth et al. 2003) and have been confirmed over North America (Ross and Elliott 1996, 2001). Unfortunately, the observations of water vapor in the atmosphere are of poor quality and suffer from changes in instrumentation over time that make detection of reliable trends difficult (Trenberth et al. 1987; Gaffen et al. 1991; Ross and

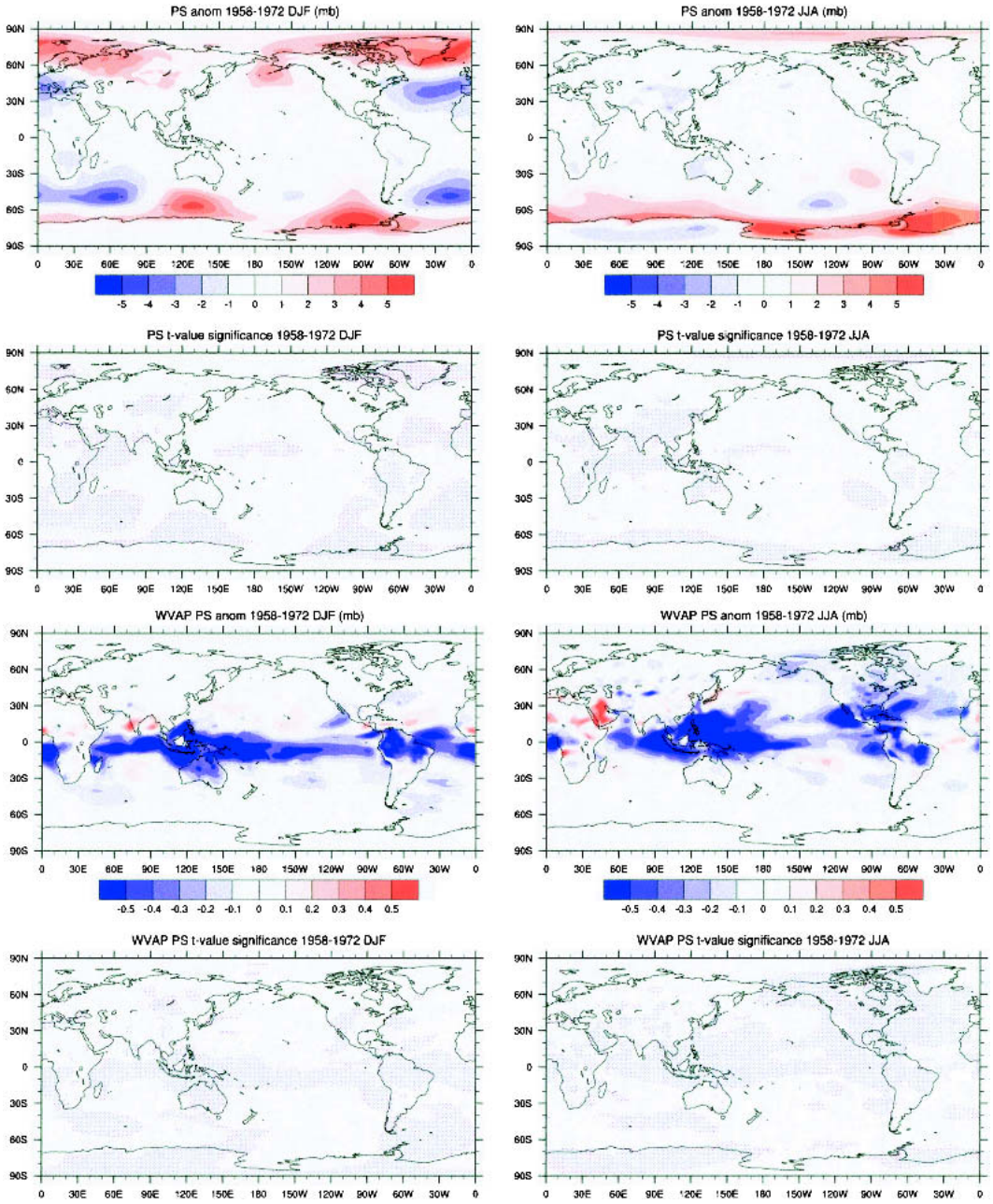

FIG. 6. Differences in means of (top four panels) p_s and (bottom four panels) p_w for 1958–72 compared to 1979–2001 in hPa (top in each group) and as t values (lower panels) for (left) DJF and (right) JJA. The latter have blue shading for significance at the 5% level and pink shading at the 10% level assuming one independent value per year.

Elliott 1996). Similarly, the global average suffers from lack of observations over vast ocean areas prior to the advent of SSM/I. Trenberth and Guillemot (1994) estimated the signal from both El Niño and from decadal trends to be about 0.05 hPa, which was masked in the previous study by the noise. In the ERA-40 reanalyses, the results seem to be improved for the post-1979 period. Accordingly, Fig. 10 shows zones from 20°N to 20°S from 1979 to 2001 as time series in more detail along with the corresponding Niño-3.4 sea surface temperature time series to indicate El Niño variability.

The 10°N–10°S p_w time series (Fig. 10) clearly shows a strong El Niño signal (the correlation coefficient with Niño-3.4 is 0.51 at zero lag and the maximum value is 0.61 with Niño-3.4 leading by 3–4 months; or 0.56 and 0.66 for the low-pass-filtered data). The main increase in water vapor is in the equatorial region from 10°N to 20°S often with compensating drier regions near 20°N.

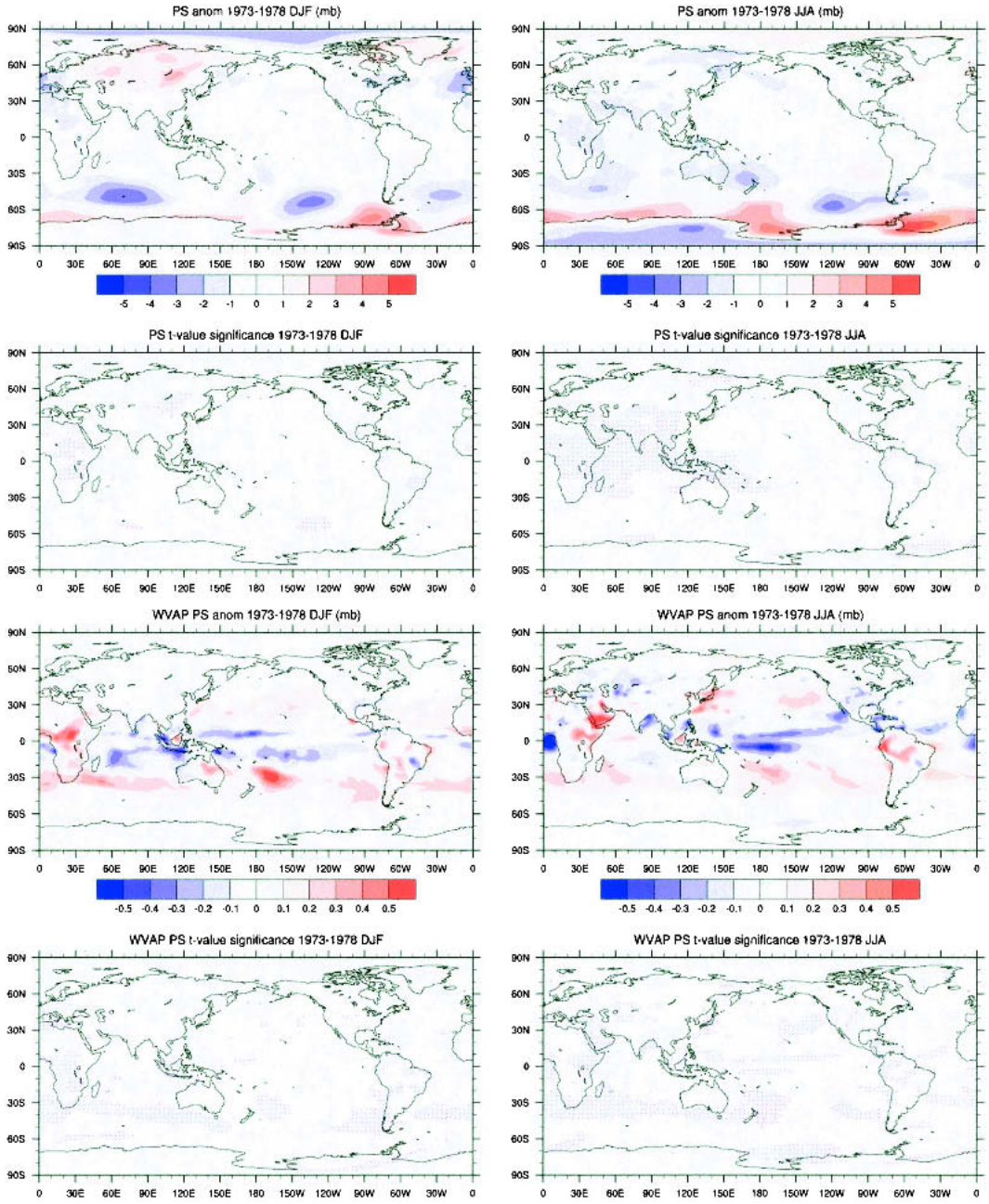

FIG. 7. Differences in means of (top four panels) p_s and (bottom four panels) p_w for 1973–78 compared to 1979–2001 in (top in each group) hPa and (bottom two panels) as t values for (left) DJF and (right) JJA. The latter have blue shading for significance at the 5% level and pink shading at the 10% level assuming one independent value per year.

In all zones the strongest relationship is with Niño-3.4 leading by 3 or 4 months, as is expected from previous studies (Trenberth et al. 2002). The correlation with the zone 10°–20°N is −0.15 at zero and 3-month lags. Hence for the Tropics as a whole (20°N–20°S), maximum correlation is 0.54 at lags of 3 and 4 months for both monthly and filtered data.

The 1982/83 and 1997/98 events show up as marked increases in moisture in the Tropics. The magnitude of the positive anomaly in p_w is on the order of 0.5 hPa (for 1982/83 and 1997/98, respectively, 0.35 and 0.49 hPa from 10°N to 10°S, 0.56 and 0.48 hPa from 10° to 20°S, and 0.24 and 0.35 hPa from 20°N to 20°S). The values from 20°N to 20°S exceed two and three standard deviations, respectively. Globally, peak monthly anomalies in p_w are 0.11 hPa for 1982/83 and 0.14 hPa

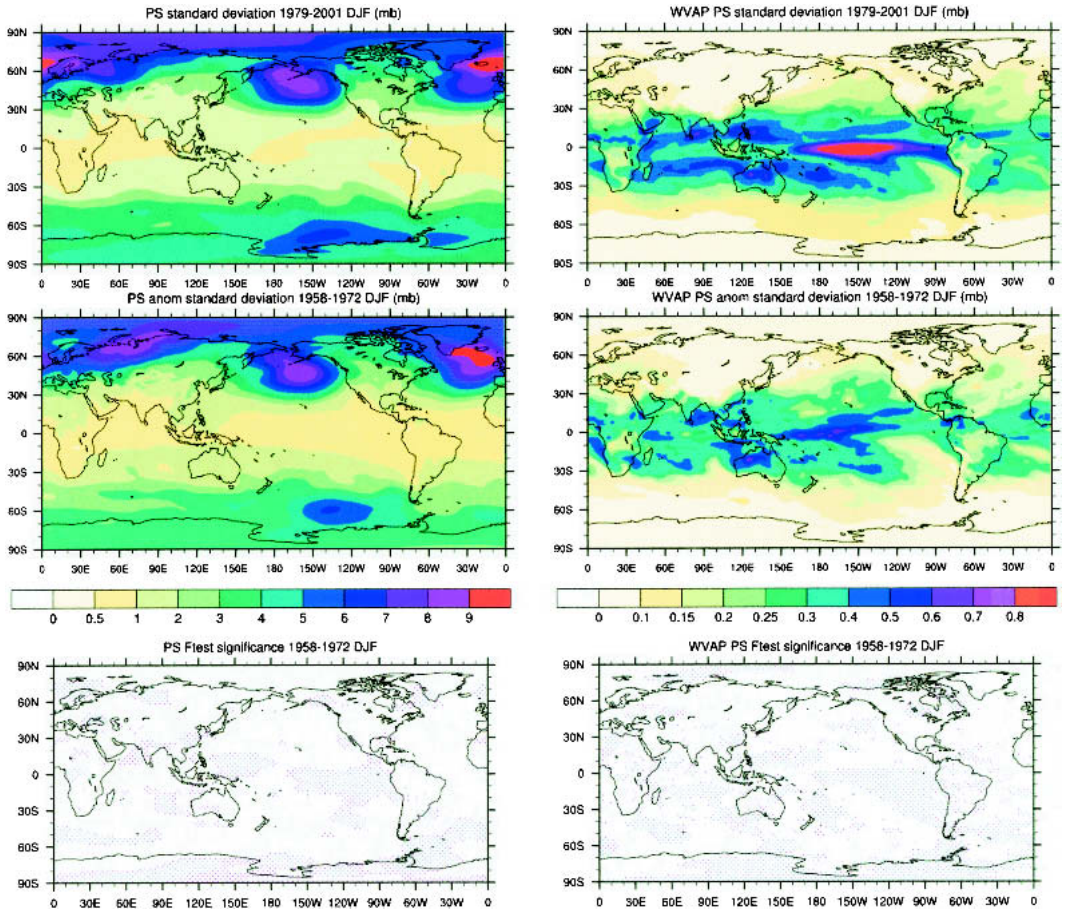

FIG. 8. Standard deviations of monthly anomalies relative to 1979–2001 means for DJF for (top) 1979–2001 and (middle) 1958–72 in hPa, and (bottom) differences significant from an *F* test assuming only one degree of freedom per year. The latter have blue shading for significance at the 5% level and pink shading at the 10% level assuming one independent value per year. (left) Surface pressures. (right) Surface pressure due to water vapor.

for 1997/98 while the lowest values occur in 1980 and 1985/86 (Fig. 2). The other El Niño events, in particular 1986–88, are less evident apparently owing to more localized effects that cancel in the zonal mean. Lowest values occur in the mid-1980s and there is some evidence for a slight upward trend. The decadal variability is likely compromised by the introduction of SSM/I data after 1986, which may also affect the interannual variability.

The eruption of Mount Pinatubo on 15 June 1991 deposited a veil of aerosol in the stratosphere and was forecast to reduce global temperatures by about 0.5°C by Hansen et al. (1992). It did so and also reduced global water vapor amounts by order 0.5 mm for precipitable water (0.05 hPa) relative to values in 1991 before the eruption (Soden et al. 2002). A minor moisture decrease is seen in the Tropics (Fig. 10) but the surface temperature decrease was mostly in the NH extratropics. Globally (Figs. 2 and 5), our results replicate those of Soden et al. (2002) reasonably well but suggest that this decrease was very minor compared with the negative anomalies from 1984 to about 1990. Nevertheless, these results may also be compromised by difficulties in properly accounting for the Pinatubo aerosol in assimilating radiances in the analyses, and this too may account for some spurious low-frequency variability.

The variability of the total mass is also a topic of considerable interest but beyond the scope of this paper. Many previous analyses exist of sea level pressure fields using techniques such as empirical orthogonal functions (EOFs) and correlation analysis to determine teleconnection patterns. Results from all of these vary somewhat and depend on details of how the analysis was carried out, such as the domain used, what grid was used, and whether values were weighted in some way. There is a significant difference in analyzing the surface pressure owing to the corrections to sea level over land, which adds a temperature-dependent artificial component to the mass (e.g., Trenberth 1981). In addition, there seems to be considerable merit in analyzing a quantity that has a global constraint of being conserved

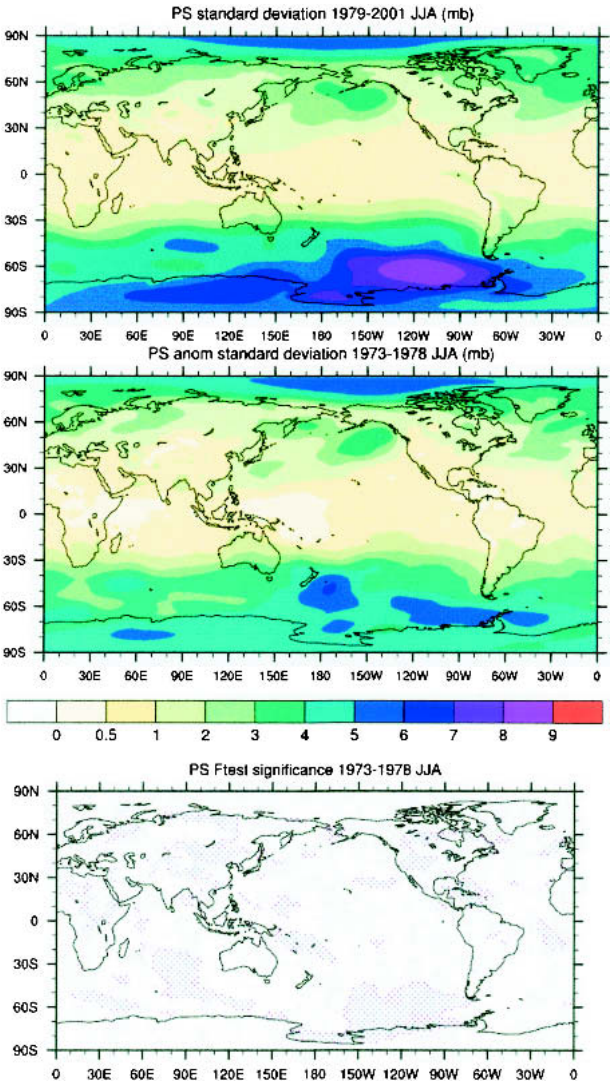

FIG. 9. Standard deviations of monthly anomalies of surface pressure in hPa relative to means of 1979–2001 for JJA for (top) 1979–2001 and (middle) 1973–78, and (bottom) the *F*-test values for differences in variance. The latter have blue shading for significance at the 5% level and pink shading at the 10% level assuming one independent value per year.

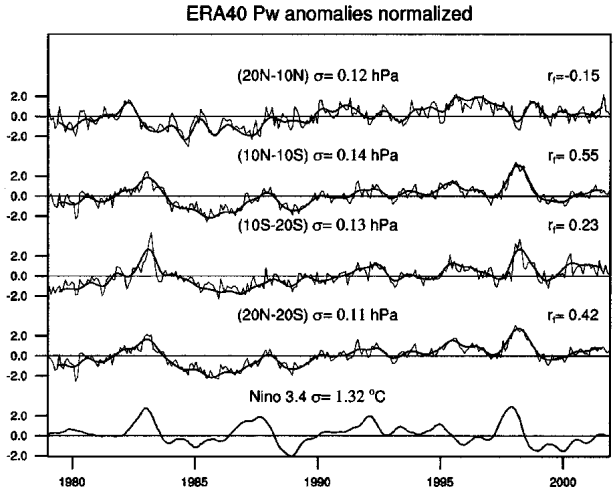

FIG. 10. Time series of monthly anomalies of p_w area averaged over zones 20°–10°N, 10°N–10°S, 10°–20°S, and 20°N–20°S, and for Niño-3.4 SSTs. In all cases the ordinate of the time series has been normalized by the standard deviation, as given. A low-pass filter has been run through the series to emphasize the interannual variability, and correlations of the filtered time series with Niño-3.4 SSTs are given at zero lag.

and thus analyzing the mass field. Relative to sea level pressure this effectively weights each value by $\cos\phi$, and thus diminishes the influence of high latitudes. These results will be reported on elsewhere.

6. Conclusions

A new estimate of global mean total mass of the atmosphere has been made based on ERA-40 data from 1979 to 2001. The dry air mass should be virtually constant to the order of 0.01-hPa surface pressure and is estimated to be $5.1352 \pm 0.0003 \times 10^{18}$ kg, corresponding to a surface pressure of 983.05 hPa. The total mean mass of the atmosphere is 5.1480×10^{18} kg corresponding to a global mean total surface pressure of 985.50 hPa, 0.9 hPa higher than previous best estimates owing to revised topography that is 5.5 m lower than previous estimates for the global mean, with the main differences coming from Antarctica. Variations in total mass occur because of changes in the water vapor loading of the atmosphere. There is a spurious annual cycle in dry air mass with a range on the order of 0.1-hPa equivalent surface pressure arising from an annual cycle of total surface pressure of 0.23 hPa that is relatively too small versus 0.29 hPa for water vapor surface pressure. Hence the range of total mass is estimated to be 1.2 to 1.5×10^{15} kg during the annual cycle as more moisture is stored in the atmosphere in northern summer, when temperatures are highest. During the 1982/83 and 1997/98 El Niño events, water vapor amounts and thus total mass increased by about 0.1 hPa in surface pressure or 0.5×10^{15} kg for several months. Some evidence exists for slight decreases following the Mount Pinatubo eruption in 1991 and also for upward trends that could be associated with increasing global mean temperatures, but uncertainties due to the changing observing system and contamination of retrievals by volcanic aerosols compromise the evidence.

We use the global constraint of constant dry air mass to evaluate the analyses. Spurious trends in both the mass of dry air and atmospheric moisture arise from changes in the observing system, especially prior to 1979 when reliable satellite data became available for global analyses. Spurious fluctuations in global mean surface pressure on the order of 0.6 hPa occur and primarily arise from low quality analyses over the South-

ern Oceans. Surface pressures are generally higher around Antarctica and contribute to global mean values on the order of 0.3 hPa higher before 1973 in ERA-40. The VTPR data, available from 1973 to 1978 improves both the mean state and cuts down on spurious variability, but is not as good as the TOVS data in this regard. It also leads to water vapor column values that are too high in the subtropics. Large disparities exist between water vapor amounts, with much lower values in the Tropics prior to 1973.

Sorting out the spurious component from real climate change and stratospheric ozone-depletion effects (Gillett and Thompson 2003) is especially difficult owing to the well-documented climate shift in 1976 (Trenberth 1990) and associated changes in the SAM over the SH. For instance, bigger and more frequent El Niño events after 1976 have altered the mean state and variability throughout the Tropics and subtropics and also changed the evolution of ENSO (Trenberth et al. 2002). It is important that observing system experiments with models should be carried out to distinguish influences of changing observing systems on the global analyses. In particular, experiments that degrade the post-1979 observations to emulate those before 1973 should be done in data assimilation, as well as sorting out effects of particular components of the observations (such as TOVS versus SSM/I versus scatterometer observations).

Acknowledgments. This research is partially sponsored by NOAA under Grant NA17GP1376. The data used were provided by ECMWF.

REFERENCES

Gaffen, D. J., T. P. Barnett, and W. P. Elliott, 1991: Space and time scales of global tropospheric moisture. *J. Climate,* **4,** 989–1008.

Gillett, N. P., and D. W. J. Thompson, 2003: Simulation of recent Southern Hemisphere climate change. *Science,* **302,** 273–275.

Hansen, J., A. Lacis, R. Ruedy, and M. Sato, 1992: Potential climate impact of Mount Pinatubo eruption. *Geophys. Res. Lett.,* **19,** 215–218.

Hoinka, K. P., 1998: Mean global surface pressure series evaluated from ECMWF reanalysis data. *Quart. J. Roy. Meteor. Soc.,* **124,** 2291–2297.

Houghton, J.T., Y. Ding, D.J. Griggs, M. Noguer, P.J. van der Linden, X. Dai, K. Maskell, and C.A. Johnson, Eds., 2001: *Climate Change 2001: The Scientific Basis*. Cambridge University Press, 881 pp.

Keeling, R. F., and S. R. Shertz, 1992: Seasonal and interannual variations in atmospheric oxygen and implications for the global carbon cycle. *Nature,* **358,** 723–727.

Renwick, J. A., and M. J. Revell, 1999: Blocking over the South Pacific and Rossby wave propagation. *Mon. Wea. Rev.,* **127,** 2233–2247.

Ross, R. J., and W. P. Elliott, 1996: Tropospheric water vapor climatology and trends over North America: 1973–93. *J. Climate,* **9,** 3561–3574.

——, and ——, 2001: Radiosonde-based Northern Hemisphere tropospheric water vapor trends. *J. Climate,* **14,** 1602–1612.

Soden, B. J., R. T. Wetherald, G. L. Stenchikov, and A. Robock, 2002: Global cooling after the eruption of Mount Pintubo: A test of climate feedback by water vapor. *Science,* **296,** 727–730.

Trenberth, K. E., 1981: Seasonal variations in global sea level pressure and the total mass of the atmosphere. *J. Geophys. Res.,* **86,** 5238–5246.

——, 1990: Recent observed interdecadal climate changes in the Northern Hemisphere. *Bull. Amer. Meteor. Soc.,* **71,** 988–993.

——, 1991: Climate diagnostics from global analyses: Conservation of mass in ECMWF analyses. *J. Climate,* **4,** 707–722.

——, and K. C. Mo, 1985: Blocking in the Southern Hemisphere. *Mon. Wea. Rev.,* **113,** 3–21.

——, and C. J. Guillemot, 1994: The total mass of the atmosphere. *J. Geophys. Res.,* **99,** 23 079–23 088.

——, J. R. Christy, and J. G. Olson, 1987: Global atmospheric mass, surface pressure, and water vapor variations. *J. Geophys. Res.,* **92,** 14 815–14 826.

——, D. P. Stepaniak, J. W. Hurrell, and M. Fiorino, 2001: Quality of reanalyses in the Tropics. *J. Climate,* **14,** 1499–1510.

——, J. M. Caron, D. P. Stepaniak, and S. Worley, 2002: Evolution of El Niño–Southern Oscillation and global atmospheric surface temperatures *J. Geophys. Res.,* **107,** 4065, doi:10.1029/2000JD000298.

——, A. Dai, R. M. Rasmussen, and D. B. Parsons, 2003: The changing character of precipitation. *Bull. Amer. Meteor. Soc.,* **84,** 1205–217.

van den Dool, H., and S. Saha, 1993: Seasonal redistribution and conservation of atmospheric mass in a general circulation model. *J. Climate,* **6,** 22–30.

Weng, F., N.C. Grody, R. Ferraro, A. Basist, and D. Forsyth, 1997: Cloud liquid water climatology from Special Sensor Microwave/Imager. *J. Climate,* **10,** 1086–1098.

Wu, W., M. Iredell, S. Saha, and P. Caplan, 1997: Changes to the 1997 NCEP MRF model analysis/forecast system. Tech. Proc. Bull. 443, Office of Meteorology, NWS, Silver Spring, MD, 22 pp.